

TOPOLOGICAL ENTROPY OF BRAIDS ON THE TORUS*

MATTHEW D. FINN[†] AND JEAN-LUC THIFFEAULT[‡]

Abstract. A fast method is presented for computing the topological entropy of braids on the torus. This work is motivated by the need to analyze large braids when studying two-dimensional flows via the braiding of a large number of particle trajectories. Our approach is a generalization of Moussafr's technique for braids on the sphere. Previous methods for computing topological entropies include the Bestvina–Handel train-track algorithm and matrix representations of the braid group. However, the Bestvina–Handel algorithm quickly becomes computationally intractable for large braid words, and matrix methods give only lower bounds, which are often poor for large braids. Our method is computationally fast and appears to give exponential convergence towards the exact entropy. As an illustration we apply our approach to the braiding of both periodic and aperiodic trajectories in the sine flow. The efficiency of the method allows us to explore how much extra information about flow entropy is encoded in the braid as the number of trajectories becomes large.

Key words. topological entropy, braid groups

AMS subject classifications. 37B40, 37M25, 20F36

1. Introduction. Investigation of two-dimensional fluid mixing by topological techniques is rapidly gaining popularity [1]. Topological perspectives on mixing either involve studying braiding motion of the stirring apparatus itself [5], or the diagnosis of mixing by analyzing braiding of orbits of the flow [10–12, 18]. The quantity that is usually of interest is the topological entropy of the braid [4], which serves as a lower bound for the topological entropy of the flow. The topological entropy of the flow is related to the exponential growth rate of material lines [17], which has long been a favorite measure of mixing quality, though it is by no means the only one [9]. In many cases the braid entropy is quite a sharp bound on the flow entropy [8, 10, 12], which is one reason why analyzing braids is useful. Another reason is that experimental particle trajectory data can be found easily by particle image velocimetry, but it is usually very difficult to measure entropies directly from material stretching or by computing Lyapunov exponents.

There are many techniques for calculating braid topological entropies, or lower bounds on them, including train-tracks [2, 13], the Burau representation of the braid group [14], and others [15, 16]. Where braiding of periodic (or aperiodic) orbits is used to analyze a flow one needs to interpret braids that have a both a large number of strands and a large number of generators. In this scenario exact methods based on train-tracks quickly become prohibitively expensive computationally, and methods based on the Burau matrix representation of the braid group usually give very poor lower bounds. Recently, however, Moussafr described a fast method for calculating the entropy of a braid to an arbitrary precision [16]. This method is based on a Dynnikov coordinate representation of a lamination [7]. In this paper we show how to extend Moussafr's technique to braids on the torus. We are motivated by the fact that many interest-

*Department of Mathematics, Imperial College London, London SW7 2AZ, United Kingdom

[†]matthew.finn@imperial.ac.uk

[‡]jeanluc@imperial.ac.uk

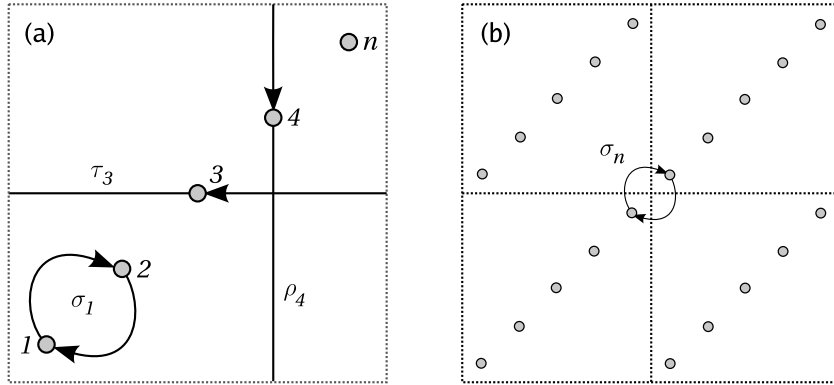


FIG. 1.1. *The spatially periodic domain with n punctures. (a) Any motion of the punctures (up to homotopy) can be written as a braid word consisting of a string of σ_i , ρ_i and τ_i motions and their inverses. (b) It is convenient to define the additional operation σ_n , the clockwise exchange of the last and first punctures.*

ing dynamical systems are defined in periodic (cylindrical or annular) or biperiodic (toroidal) spatial domains. For instance, the alternating sine flow [10] can be analyzed from a topological perspective using this approach.

Figure 1.1 shows the setting for the dynamical system under study. We consider a flow on a torus, so that the domain is periodic in both directions. We identify n distinguished points that we call punctures. We then consider motions that move the punctures in such a way that they always return to their initial configuration, possibly having been permuted amongst themselves. The three types of motions that we consider are illustrated in Figure 1.1(a); they are

1. σ_i , the clockwise interchange of the i th and $(i + 1)$ th puncture;
2. ρ_i , the i th puncture making a full tour around the vertical periodic direction;
3. τ_i , the i th puncture making a full tour around the horizontal periodic direction.

The inverse of any of these motions is obtained by reversing its direction. The elementary motions $\{\sigma_i, \rho_i, \tau_i\}$ are generators of the braid group on n strands on the torus [3]. Recognizing the periodicity of the domain, we also define an additional operation σ_n to be the clockwise interchange of the n th puncture with the first puncture. To be precise, we mean here the first puncture in the ‘copy’ of the domain above and to the right of the n th puncture, as pictured in Figure 1.1(b), so that both periodic boundaries are crossed in performing σ_n . Defining σ_n in this way keeps both periodic directions on an equal footing, and is also convenient in what follows as it is related to a translational symmetry for the punctures.

A sequence of generators, such as $\rho_3^{-1}\sigma_2\rho_6\sigma_6$, is called a braid word, and we use the convention that the elementary motions in a braid word occur from left to right, so that ρ_3^{-1} occurs first in our example. By *planar braid* we mean a braid word that can be written using only generators from the set $\{\sigma_1, \dots, \sigma_{n-1}\}$, and their inverses. A planar braid is equivalent to a braid on the plane with n punctures. In other words, a planar braid does not take advantage of the periodic directions. By *cylinder braid* (or annular braid) we mean a braid word that can be written using only generators

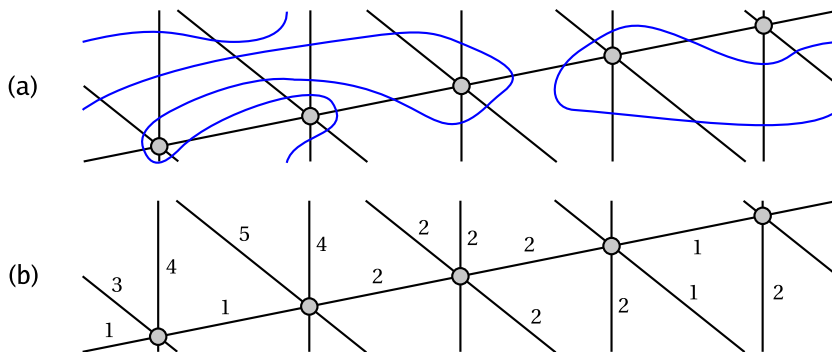


FIG. 2.1. (a) A representative curve of a lamination on a toroidal domain with five punctures. The top and bottom edges, and the left and right edges, are identified so that the picture shows exactly ten triangles. (b) The number of crossings with each edge of the triangulation, from which the lamination can be reconstructed.

from either the set $\{\sigma_1, \dots, \sigma_{n-1}, \rho_1, \dots, \rho_n\}$ or $\{\sigma_1, \dots, \sigma_{n-1}, \tau_1, \dots, \tau_n\}$, and their inverses. In other words, a cylinder braid takes advantage of one periodic direction, but not the other. Finally, a *torus braid* is a braid word that is neither a planar braid nor a cylinder braid. In this paper we will derive a general method for torus braids, which includes planar and cylinder braids as special cases.

The description of our method here is intended to be accessible to dynamicists and requires no specialist understanding of braid groups. The paper is divided as follows. In the following section we describe how laminations (equivalence classes of simple closed curves) can be encoded by triangulation of the flow domain. Section 3, the heart of the paper, gives the details of how this encoding evolves under fundamental braiding actions or motions. Several examples are given in Section 4 to illustrate and verify the method. In Section 5 we show how to compute the topological entropy from evolution of laminations, and demonstrate the rapid convergence. We also look at braiding in the sine flow as an example application. We summarize our work in Section 6 and discuss some features and possibilities for further study.

2. Encoding of laminations by triangulation. We wish to calculate a lower bound on how rapidly material lines are stretched in a continuous-time flow based on the motion of a finite number of punctures, or a finite set of periodic orbits. Our approach, inspired by the method of Moussafir [16], is to study the stretching and folding of laminations. A lamination is an equivalence class (under homotopy) of simple closed curves that are not homotopic to any part of the boundary (treating the punctures as boundaries), and cannot be continuously shrunk to a point. For example, a loop that encloses at least two punctures belongs to a lamination. We usually represent a lamination by drawing one loop in the equivalence class. An example of a lamination on our doubly-periodic toroidal domain is shown in Figure 2.1(a).

In order to calculate how a given lamination is transformed under the action of the braid, it is necessary to have a way of encoding the lamination, and a method for evolving this encoding under the action of the braid. An elegant way of encoding the lamination is by triangulating the entire domain and counting the number of crossings the lamination makes with the edges of the triangulation. The number of crossings for our example lamination is shown in Figure 2.1(b). Note that there are

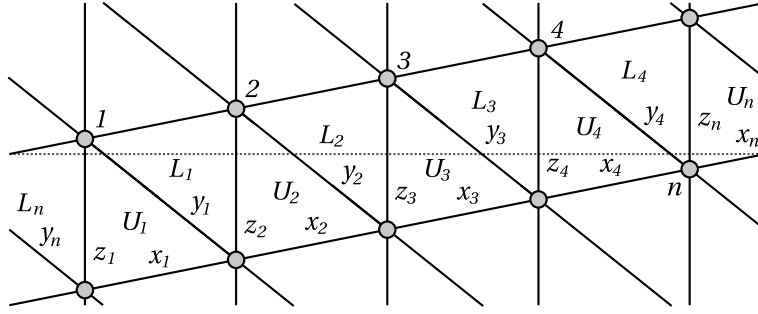


FIG. 2.2. Notation for our chosen triangulation of the doubly periodic domain with n punctures. The domain is divided into $2n$ triangles U_i and L_i . Two copies of the domain are shown one above the other for clarity. The $3n$ numbers x_i , y_i and z_i are used to count how many crossings a lamination makes with each edge of the triangulation. The lamination is assumed to be pulled tight, which means that when the curve enters a triangle it must leave through a different edge to the one it entered by. Note that this triangulation is not unique, but is chosen for convenience in the calculations that follow.

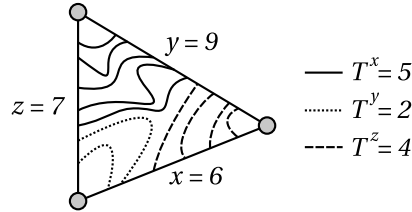


FIG. 2.3. The lamination inside a triangle T (where T is U_i or L_i from Figure 2.2) can be completely reconstructed from the set of crossing numbers $\{x_i, y_i, z_i\}$. To construct the solution, each triangle is solved separately, and the triangles are patched together in the obvious way. The solution in a single triangle is illustrated. Equation (2.1) determines the number of curves that must pass directly between each pair of edges. Up to homotopy, there is only one way to draw these curves without crossings.

infinitely many different ways the domain can be triangulated, so in this paper we choose a triangulation that is most convenient for studying the action of braiding motions. The notation we use for counting crossings is illustrated in Figure 2.2. For n punctures the resulting encoding $\{x_i, y_i, z_i\}$ contains $3n$ crossing numbers.

To ensure that each homotopic lamination produces the same set of crossings we insist that the lamination is first pulled tight, which means that no loops are allowed where the lamination enters and leaves a triangle by the same edge. Under the pulled-tight assumption, the set of crossing numbers uniquely identifies the lamination. The reason for this is that the path of the lamination can be determined uniquely in each triangle, and therefore the global solution is found to be unique by patching the triangles together. The unconvinced reader is invited to attempt to find any other solution for the given crossing numbers that is not homotopic to the lamination shown in Figure 2.1.

To draw the lamination from the set of crossing numbers we explain the solution procedure for each triangle. Consider the triangle T depicted in Figure 2.3, where T is U_i or L_i from Figure 2.2. The crossing numbers with each of the three edges are x , y and z . In our notation, any part of the lamination passing between edges x and y is

counted by T^z , and, likewise, T^y counts lines passing between x and z and T^x counts lines between y and z . Since we assume the lamination is pulled tight at all times, there cannot be any lines that enter and leave by the same edge, so $T^x + T^y + T^z$ counts all the lines. A simple bit of bookkeeping shows we must have $x = T^y + T^z$, $y = T^x + T^z$ and $z = T^x + T^y$, which gives

$$\begin{aligned} T^x &= \frac{1}{2}(y + z - x), \\ T^y &= \frac{1}{2}(x + z - y), \\ T^z &= \frac{1}{2}(x + y - z). \end{aligned} \tag{2.1}$$

Given T^x , T^y and T^z , there is then only one way to draw the lines without them crossing each other. The T^x , T^y and T^z lines are highlighted using different dash patterns for the example in Figure 2.3. The numbers given by (2.1) are crucial to the arguments that follow.

3. Deformation of laminations under braid operations. In this section we describe the effect of braiding operations on a lamination. We start with a lamination that is pulled tight, and we record the initial set of crossing numbers $\{x_i, y_i, z_i\}$. All we have to do now is to determine how these numbers are updated under the action of each braid operation.

To calculate the new set of crossings we simply determine the number of crossings with the *preimage* of each edge. We denote the preimage of edge e by e^* , which is a curve that becomes e (up to homotopy) after the braid operation. Our argument is that the number of crossings of e^* before the braid operation has to be equal to the number of crossings with e afterwards. This must be the case, as the only way the number of crossings could change is if the end of a loop were to cross through the edge as it is deformed from e^* to e — but by the pulled-tight assumption any such loop would have to be wrapped around a puncture, and by construction no punctures pass through the edge as it deforms from e^* to e .

It will turn out that we only have to consider explicitly the braid group operations ρ_i, ρ_i^{-1} ($i = 1, \dots, n$) and σ_i, σ_i^{-1} ($i = 1, \dots, n - 1$). We then determine the effect of other independent group elements τ_i and τ_i^{-1} by invoking group presentation rules and the operation σ_n (see Figure 1.1(b)). This is explained in detail in Section 3.5 for those not familiar with the braid group presentation. For convenience we assume in what follows that indices are treated ‘modulo’ n , so that the puncture to the right of puncture n is puncture 1.

3.1. Crossing update rules for ρ_i . For the braid operation ρ_i , we need only consider edges incident on the i th puncture, since the number of crossings with other edges will remain unchanged. The relevant preimages are shown in Figure 3.1 as dashed lines. Many of the preimages are other edges (e.g. x_{i-1} is the preimage y_{i-1}^*), so the number of crossings is already known. This is not a coincidence: the triangulation was chosen for this property. The two preimages x_{i-1}^* and y_i^* require a little more attention. In Figure 3.2 we illustrate that the number of crossings x_{i-1}^* can be calculated by a simple bookkeeping argument. The number of crossings y_i^* can be deduced in a similar way.

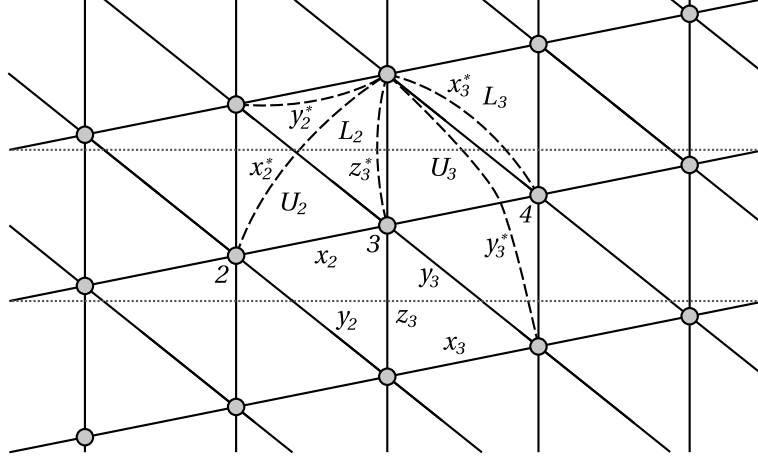


FIG. 3.1. Preimage illustration for ρ_3 . Only edges that are incident with the moving puncture can have a change in crossing number. For ρ_3 the five edges are x_2 , y_2 , x_3 , y_3 and z_3 . In this example x_2 and y_3 are the exact preimages of y_2 and x_3 , respectively. The edge z_3 is the preimage of itself, so in fact its crossing number will not change under ρ_3 . The preimages of x_2 and y_3 are not edges in the triangulation, so more work is required to determine how many crossings are made, as shown in Figure 3.2.

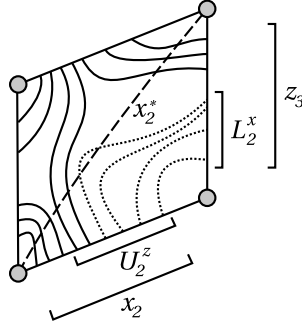


FIG. 3.2. The number of crossings with a preimage that is not part of the triangulation may be found by simple bookkeeping. We illustrate here how to determine the number of crossings with the x_2^* preimage. All curves entering x_2 and z_3 must cross x_2^* (by the pulled-tight assumption), unless they loop directly from x_2 to z_3 (shown dotted). The number of these loops is exactly $\min(U_2^z, L_2^x)$. Hence the number of preimage crossings is $x_2 + z_3 - 2 \min(U_2^z, L_2^x)$. Note that curves that cross over the preimage and immediately back again are automatically discounted, so that the pulled-tight assumption still holds for the updated set of crossing numbers.

The update rules for all the edges considered are

$$\begin{aligned}
 x_{i-1}^* &= x_{i-1} + z_i - 2 \min(U_{i-1}^z, L_{i-1}^x) = x_{i-1} + z_{i-1} - 2 \min(U_{i-1}^x, L_{i-1}^z), \\
 y_{i-1}^* &= x_{i-1}, \\
 x_i^* &= y_i, \\
 y_i^* &= z_i + y_i - 2 \min(U_i^y, L_i^z) = y_i + z_{i+1} - 2 \min(U_i^z, L_i^y), \\
 z_i^* &= z_i.
 \end{aligned} \tag{3.1}$$

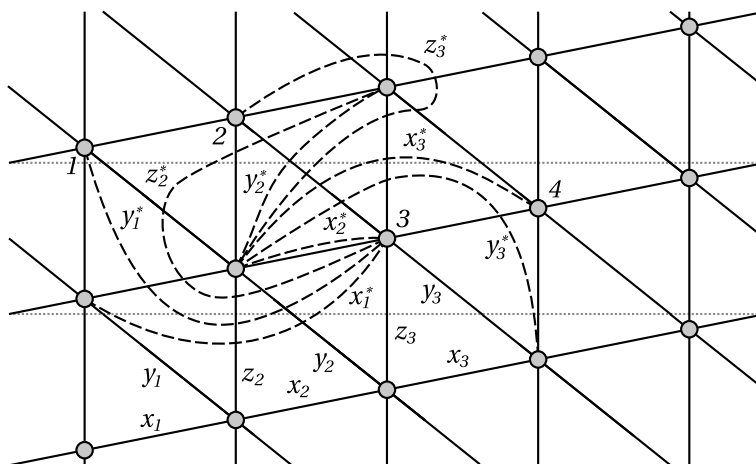


FIG. 3.3. *Preimage illustration for σ_2 . The dashed lines show the preimages of all edges whose crossing number may change. Edge x_2 is its own preimage, but all other preimages require some bookkeeping. Figure 3.4 illustrates how to compute the crossings with x_1^* and y_1^* . Computation of y_2^* is done as in Figure 3.2. Preimages x_3^* and y_3^* are handled in the same way as x_1^* and y_1^* , by invoking rotational symmetry. The difficult preimage problems are z_2^* and z_3^* , as these preimages cross through seven triangles; the solution is described in Section 3.3.*

3.2. Crossing update rules for ρ_i^{-1} . We can work out the update rule for ρ_i^{-1} by noting the π -rotational symmetry of the triangulation about a puncture and relabelling the variables in the rules (3.1) given above. The update rules for affected crossing numbers are

$$\begin{aligned}
 x_{i-1}^* &= y_{i-1}, \\
 y_{i-1}^* &= y_{i-1} + z_i - 2 \min(U_{i-1}^z, L_{i-1}^y) = y_{i-1} + z_{i-1} - 2 \min(U_{i-1}^y, L_{i-1}^z), \\
 x_i^* &= z_i + x_i - 2 \min(U_i^x, L_i^z) = x_i + z_{i+1} - 2 \min(U_i^z, L_i^x), \\
 y_i^* &= x_i, \\
 z_i^* &= z_i.
 \end{aligned} \tag{3.2}$$

3.3. Crossing update rules for σ_i . The same ideas can be used to determine the updated crossing numbers following a σ_i operation. However, since there are two moving punctures, more edges are affected, and the preimages are therefore more complicated. An example of a preimage diagram for σ_2 is shown in Figure 3.3. In general, for σ_i the affected crossing numbers are x_{i-1} , y_{i-1} , x_i , y_i , z_i , x_{i+1} , y_{i+1} and z_{i+1} . This includes the operation σ_n which switches the first and last punctures across the periodic boundaries (see Figure 1.1(b)); we shall require this operation in Sections 3.5–3.6 to find the update rules for τ_i and τ_i^{-1} .

The edge x_i is its own preimage, and the number of crossings with y_i^* is determined using the quadrilateral trick illustrated in Figure 3.2. The number of crossings with x_{i-1}^* , y_{i-1}^* , x_{i+1}^* and y_{i+1}^* can be found by extending the quadrilateral solution over three and four triangles, as illustrated in Figure 3.4.

The two remaining crossing numbers to find are z_i^* and z_{i+1}^* . Since these preimages pass through a total of seven triangles it is non-trivial to determine the number of crossings directly. Instead we employ a trick and deduce z_i^* and z_{i+1}^* by invoking

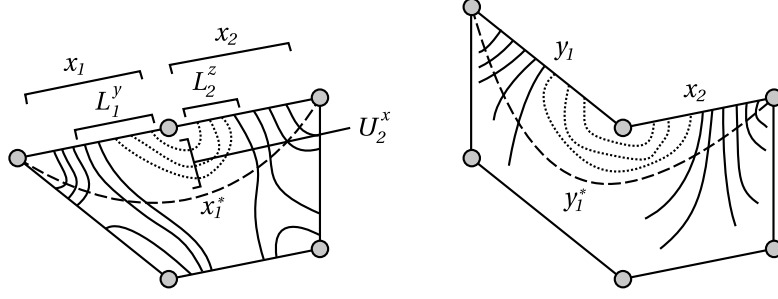


FIG. 3.4. Two slightly more difficult preimage puzzles for the operation σ_2 . In a similar way to in Figure 3.2, the number of crossings with preimage x_1^* is given by the number of curves crossing x_1 and x_2 , minus twice the number of loops directly between x_1 and x_2 . The number of such loops is exactly $\min(L_1^y, U_2^x, L_2^z)$. Hence $x_1^* = x_1 + x_2 - 2\min(L_1^y, U_2^x, L_2^z)$. The preimage problem for y_1^* is similar, but involves four triangles and hence a minimum of four numbers, so that $y_1^* = y_1 + x_2 - 2\min(U_1^z, L_1^y, U_2^x, L_2^z)$.

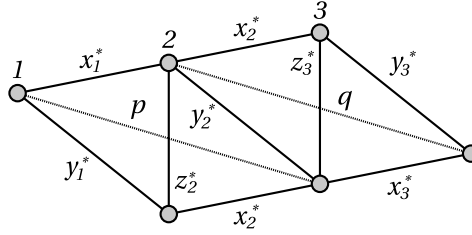


FIG. 3.5. The number of crossings with z_i^* and z_{i+1}^* are difficult to determine directly from the old set of crossing numbers. However they may be calculated using the quadrilateral solution shown in Figure 3.2 from the already updated crossing numbers.

the quadrilateral solution again with the *updated* crossing numbers. We introduce temporary edges p and q directly between punctures $i-1$ and $i+1$ and between i and $i+2$, as shown in Figure 3.5. The preimage of p is y_{i-1} , and the preimage of q is y_{i+1} . Since x_{i-1}^* , y_{i-1}^* , p , x_i^* , y_i^* , q , x_{i+1}^* and y_{i+1}^* are known, z_i^* and z_{i+1}^* can be deduced easily.

The collected update rules for the affected crossing numbers are

$$\begin{aligned}
 x_{i-1}^* &= x_{i-1} + x_i - 2\min(L_{i-1}^y, U_i^x, L_i^z), \\
 y_{i-1}^* &= y_{i-1} + x_i - 2\min(U_{i-1}^z, L_{i-1}^y, U_i^x, L_i^z), \\
 x_i^* &= x_i, \\
 y_i^* &= z_i + x_i - 2\min(U_i^x, L_i^z) = x_i + z_{i+1} - 2\min(U_i^z, L_i^x), \\
 z_i^* &= x_{i-1}^* + y_{i-1}^* - \min(y_{i-1}^* + y_{i-1} - x_i^*, x_{i-1}^* + y_{i-1} - y_i^*), \\
 x_{i+1}^* &= x_i + x_{i+1} - 2\min(U_i^z, L_i^x, U_{i+1}^y), \\
 y_{i+1}^* &= x_i + y_{i+1} - 2\min(U_i^z, L_i^x, U_{i+1}^y, L_{i+1}^z), \\
 z_{i+1}^* &= x_i^* + y_i^* - \min(x_i^* + y_{i+1} - y_{i+1}^*, y_i^* + y_{i+1} - x_{i+1}^*).
 \end{aligned} \tag{3.3}$$

3.4. Crossing update rules for σ_i^{-1} . Since the triangulation does not have a reflection symmetry about a vertical line through the midpoint of two punctures, it is not possible to deduce the update rules for σ_i^{-1} by a relabelling in the rules for

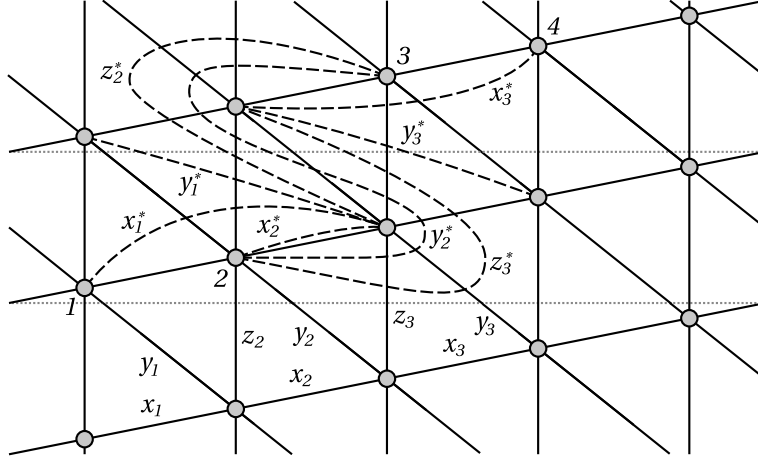


FIG. 3.6. Preimage illustration for σ_2^{-1} . Note that due to asymmetry the preimage problems are slightly different to those for σ_2 .

σ_i . An example of a preimage diagram for σ_2^{-1} is shown in Figure 3.6. The preimage curve y_i^* is the most complicated yet, as it passes through ten triangles. However the crossing number of all these preimages can be calculated as before using the techniques illustrated in Figures 3.2, 3.4 and 3.5.

The update rules for the affected crossing numbers are

$$\begin{aligned}
 x_{i-1}^* &= x_{i-1} + x_i - 2 \min(U_{i-1}^z, L_{i-1}^x, U_i^y), \\
 y_{i-1}^* &= y_{i-1} + x_i - 2 \min(L_{i-1}^x, U_i^y) = x_{i-1} + y_i - 2 \min(L_{i-1}^y, U_i^x), \\
 x_i^* &= x_i, \\
 y_i^* &= x_i^* + z_i^* - \min(z_i^* + y_i - x_i^*, x_i^* + y_i - z_{i+1}^*), \\
 z_i^* &= x_i + y_i - 2 \min(U_i^x, L_{i-1}^y, U_{i-1}^z, L_{i-1}^x, U_i^y), \\
 x_{i+1}^* &= x_i + x_{i+1} - 2 \min(L_i^y, U_{i+1}^x, L_{i+1}^z), \\
 y_{i+1}^* &= y_i + x_{i+1} - 2 \min(L_i^x, U_{i+1}^y) = x_i + y_{i+1} - 2 \min(L_i^y, U_{i+1}^x), \\
 z_{i+1}^* &= x_i + y_i - 2 \min(L_i^y, U_{i+1}^x, L_{i+1}^z, U_{i+1}^y, L_i^x).
 \end{aligned} \tag{3.4}$$

3.5. Crossing update rules for τ_i . In Sections 3.1-3.4 we showed how to update the set of crossing numbers $\{x_i, y_i, z_i\}$ for the braid operations $\rho_i, \rho_i^{-1}, \sigma_i$ and σ_i^{-1} . To complete the set of update rules for any braid we must give the corresponding rules for τ_i and τ_i^{-1} . In performing τ_i the i th puncture moves once around the torus in the horizontal direction (see Figure 1.1). In doing so it passes through many edges in our triangulation, so it is difficult to draw the preimages and to derive the number of crossings directly. However, we can deduce the update rules for τ_i and τ_i^{-1} by appealing to group properties that relate σ_i, ρ_i and τ_i . In Figure 3.7 we illustrate how τ_1 is achieved through a sequence of σ_i^{-1} (including σ_n^{-1} defined in Figure 1.1(b)) followed by one ρ_1^{-1} . The other τ_i and τ_i^{-1} are produced in a similar manner. A computational recipe for each τ_i operation is given in this section, and τ_i^{-1} in the following section.

To calculate the updated set of crossing numbers $\{x_i, y_i, z_i\}$ for τ_i do the following:

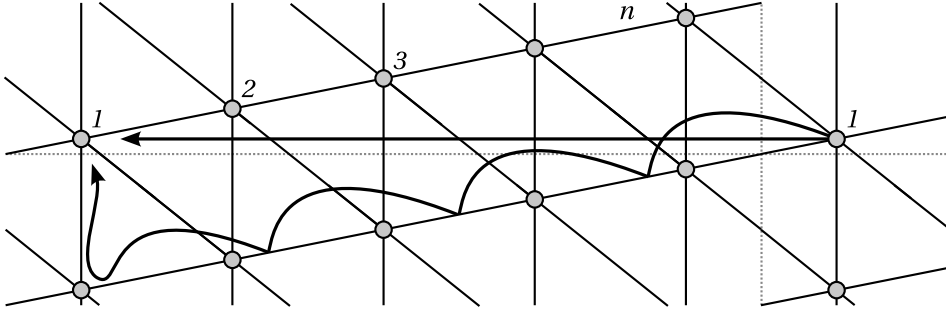


FIG. 3.7. The operation τ_1 is achieved using a sequence of σ_j^{-1} operations, including the operation σ_n^{-1} (see Figure 1.1), followed by a single ρ_1^{-1} . This is described in more detail in the text.

1. Use equation (3.4) to perform, in turn, $\sigma_{i-1}^{-1}, \sigma_{i-2}^{-1}, \dots, \sigma_{i+2}^{-1}$ and σ_{i+1}^{-1} . Treat the indices ‘modulo’ n , so that σ_n^{-1} follows σ_1^{-1} .
2. Relabel $x_i \leftarrow x_{i+1}, y_i \leftarrow y_{i+1}$ and $z_i \leftarrow z_{i+1}$. This leaves all punctures except the i th one in the correct position.
3. Use equation (3.2) to perform ρ_i^{-1} .

3.6. Crossing update rules for τ_i^{-1} . To calculate the updated set of crossing numbers $\{x_i, y_i, z_i\}$ for τ_i^{-1} invert the operation of Section 3.5 as follows:

1. Use equation (3.1) to perform ρ_i .
2. Relabel $x_i \rightarrow x_{i+1}, y_i \rightarrow y_{i+1}$ and $z_i \rightarrow z_{i+1}$. This leaves the punctures in the wrong position, but the next sequence corrects everything...
3. Use equation (3.3) to perform, in turn, $\sigma_{i+1}, \sigma_{i+2}, \dots, \sigma_{i-2}$ and σ_{i-1} . Treat the indices ‘modulo’ n , so that σ_1 follows σ_n .

4. Illustrations using simple braids. To illustrate the use of the update rules given in Section 3 we show how a lamination is deformed under some simple previously studied braids. We have implemented the update rules in a short C++ program, using the Gnu Multiple Precision library to allow the number of crossings to grow arbitrarily large whilst maintaining exact arithmetic. We also have a Matlab script to draw the lamination, one triangle at a time, using the procedure described in Section 2. This was used to produce all the figures in this section. In each case our initial lamination is a closed loop that passes between the first two punctures, with $x_1 = y_1 = 1$ and all other x_i, y_i and z_i set to zero (see the upper-left frame in Figure 4.1).

Figure 4.1 shows the roll up of the lamination under the repeated action of the planar braid σ_1 with three punctures. In this case it is clear that the third puncture is redundant. This braid has zero entropy and is very poor at stirring as it results in linear growth of material lines. Note that even though coils form around the pair of moving punctures there is always exactly one crossing of the lamination from one copy of the domain to the copy above. This is because there was exactly one crossing in the initial lamination and this is only a planar braid, so it cannot create any further crossings under the pulled-tight assumption.

Figure 4.2 shows the result of repeating τ_2 with three punctures. In this simple braid the second puncture moves in a straight line to the left, but catching the lamination

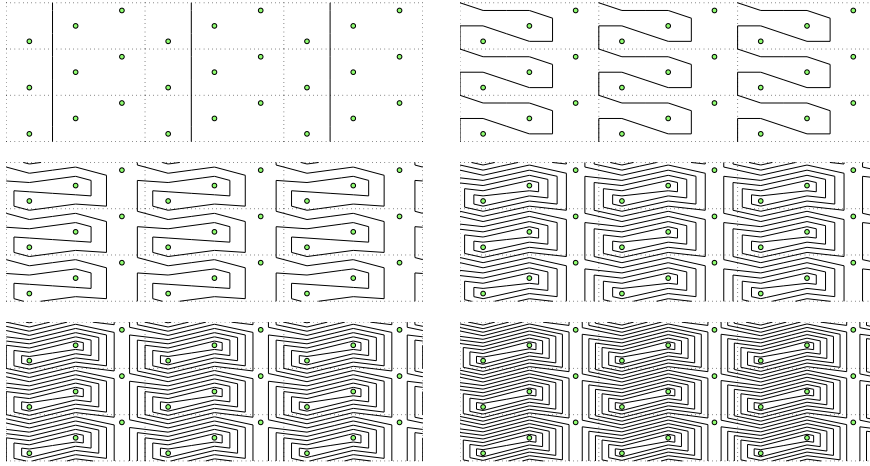


FIG. 4.1. Lamination evolution under the braid σ_1 . This results in linear growth in the number of crossings, and zero entropy.

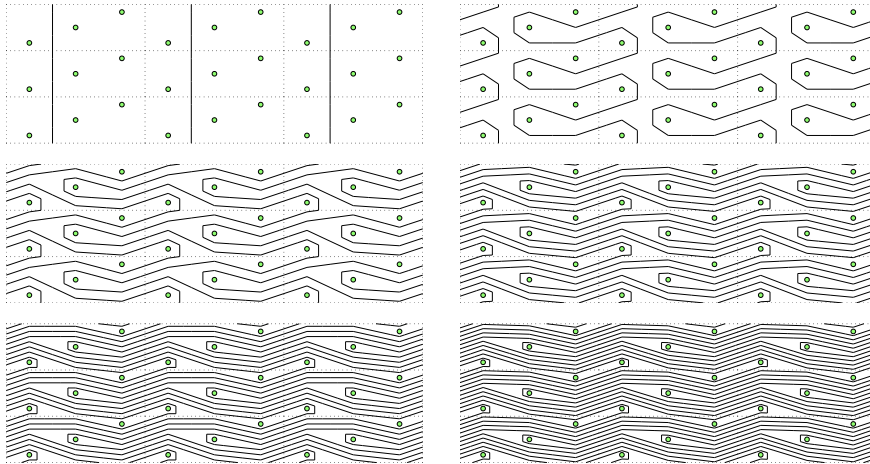


FIG. 4.2. Lamination evolution under the braid τ_2 . This braid also has zero topological entropy, but the illustration is provided to verify the correctness of the procedure for performing τ using a combination of σ and ρ .

on the puncture exactly once. The illustration is provided to validate the method described in Sections 3.5–3.6 for performing τ operations using a combination of σ and ρ motions.

The planar pigtail braid $\sigma_1\sigma_2^{-1}$ with three punctures is illustrated in Figure 4.3 [5]. This braid is pseudo-Anosov and has a growth rate per braid letter of $\frac{1}{2}(1 + \sqrt{5})$, which is the golden ratio. This ‘golden braid’ has been proved to have the highest topological entropy per braid letter for a planar braid [6].

Figure 4.4 illustrates a related cylinder braid $\sigma_1\sigma_3\sigma_2^{-1}\sigma_4^{-1}$ with four punctures. This is similar to the pigtail braid but wrapped around a cylinder so that the first and last punctures are allowed to exchange places. The cylinder braid $\sigma_1\sigma_2^{-1}$ with *two* punctures has a growth rate per braid letter given by the silver ratio of $1 + \sqrt{2}$, and

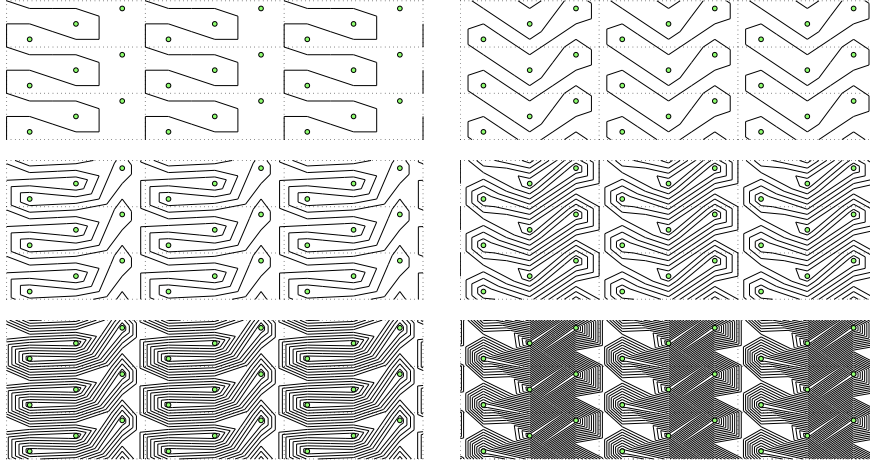


FIG. 4.3. Lamination evolution under the (planar) golden braid $\sigma_1\sigma_2^{-1}$. This braid is proved to have highest topological entropy per braid letter for a planar braid [6].

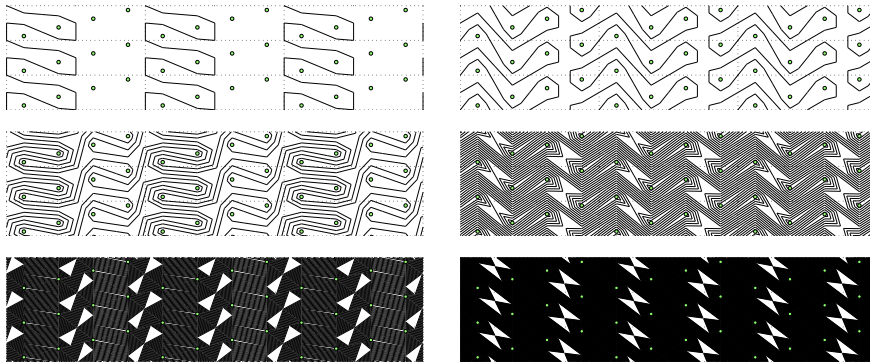


FIG. 4.4. Lamination evolution under the cylinder braid $\sigma_1\sigma_3\sigma_2^{-1}\sigma_4^{-1}$. Note that the lamination becomes visibly dense more quickly than for the golden braid in Figure 4.3.

this can be proved to be the optimum per braid letter over all cylinder braids. (The proof follows that of D'Alessandro [6] using a matrix representation for the cylinder braid group.) The silver braid entropy is almost fifty percent higher than the golden braid entropy, showing that periodic boundary conditions can be exploited to enhance chaos. The extra stretching is clearly visible by comparing Figures 4.3 and 4.4.

A final validation of our encoding and update rules is given by checking that any lamination is unchanged when it is subjected to the identity braid. For the braid group on the torus, one way of writing the identity using σ , ρ and τ is $\sigma_1^{-2}\rho_1^{-1}\tau_2\rho_1\tau_2^{-1}$ which is taken from the group presentation written down by Birman [3]. In Figure 4.5 the evolution of our test lamination is shown using this braid, and it is unchanged, as required.

5. Calculating topological entropies from laminations. Having completed the description of the dynamical system for deformation of a lamination, we now discuss how the topological entropy of a braid is related to evolution of a lamination. The

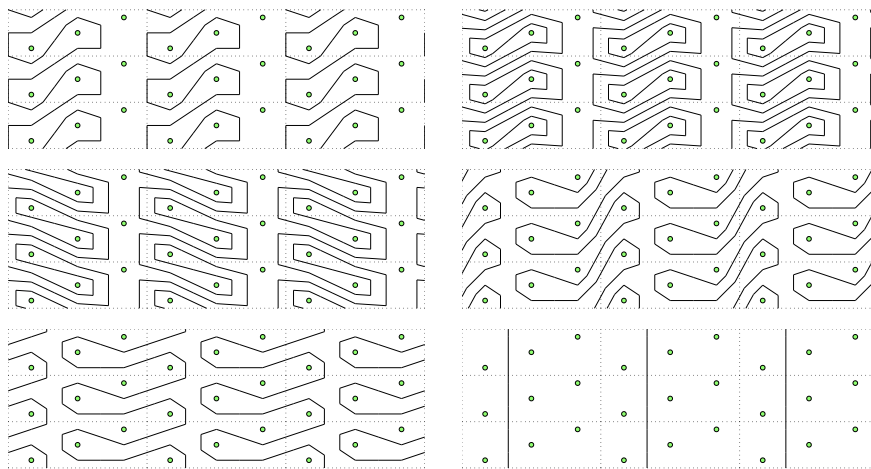


FIG. 4.5. Lamination evolution under the toroidal identity braid $\sigma_1^{-2} \rho_1^{-1} \tau_2 \rho_1 \tau_2^{-1}$. The initial lamination (not shown) is the vertical line between the first two punctures. The images show, in order, the lamination after σ_1^{-1} , σ_1^{-2} , $\sigma_1^{-2} \rho_1^{-1}$, $\sigma_1^{-2} \rho_1^{-1} \tau_2$, $\sigma_1^{-2} \rho_1^{-1} \tau_2 \rho_1$ and $\sigma_1^{-2} \rho_1^{-1} \tau_2 \rho_1 \tau_2^{-1}$. The final lamination is the same as the initial lamination, as required.

results of Moussaïf [16] for the punctured sphere apply here: for an appropriate lamination, the growth rate of the total number of crossings between the lamination and triangulation converges to the topological entropy the braid λ^\dagger . Thus, asymptotically we have the estimate

$$\lambda^\dagger = \log \sum_i (x_i^* + y_i^* + z_i^*) - \log \sum_i (x_i + y_i + z_i), \quad (5.1)$$

where the starred variables are the updated crossing numbers described in Section 3. Convergence of λ^\dagger to the exact braid entropy λ appears to be exponential (provided the braid has a pseudo-Anosov component), and so in practice very few iterations are required to obtain λ to double precision. Finite-order braids, which have zero topological entropy are detected easily by checking for sub-exponential convergence of λ^\dagger .

As an example, the exact topological entropy of the four-strand braid $\sigma_1 \sigma_3 \sigma_2^{-1} \sigma_4^{-1}$ (see the previous section and Figure 4.4) is known to be twice the logarithm of the silver ratio $\lambda = 2 \log(1 + \sqrt{2}) = 1.762747174039086\dots$. In Table 5.1 we show how the total crossing number and the entropy estimate λ^\dagger given by (5.1) evolve under the first few iterations of the braid (using the initial lamination described in Section 4). Double precision accuracy of the entropy, which is sufficient for most purposes, is reached after about 20 iterations.

Braids quite naturally arise when considering periodic trajectories of points in a two-dimensional flow. For a spatially-periodic flow the space-time plot of these trajectories is typically a cylinder or a torus braid, and the entropy of this braid provides a rigorous lower bound on the topological entropy of the flow [4,5]. Finn et al. [10] derived such a lower bound for the sine flow using Thurston's 'iterate and guess' method to construct the train-track for the braid formed by a set of periodic orbits. We will now describe how the same result can be found using our lamination approach.

The sine flow is a time-periodic alternating shear-flow defined on the unit torus

| iteration | total crossings | entropy λ^\dagger | error $ \lambda - \lambda^\dagger $ |
|-----------|------------------|---------------------------|-------------------------------------|
| 1 | 24 | 2.48490664978800 | 0.72215947574891 |
| 2 | 154 | 1.85889877206568 | 0.09615159802660 |
| 3 | 912 | 1.77868738766070 | 0.01594021362162 |
| 4 | 5330 | 1.76546652708556 | 0.00271935304647 |
| 5 | 31080 | 1.76321328732169 | 0.00046611328261 |
| 6 | 181162 | 1.76282713309230 | 0.00007995905321 |
| 7 | 1055904 | 1.76276089245107 | 0.00001371841199 |
| 8 | 6154274 | 1.76274952773491 | 0.00000235369583 |
| 9 | 35869752 | 1.76274757786911 | 0.00000040383002 |
| 10 | 209064250 | 1.76274724332535 | 0.00000006928627 |
| 11 | 1218515760 | 1.76274718592673 | 0.00000001188765 |
| 12 | 7102030322 | 1.76274717607868 | 0.00000000203960 |
| 13 | 41393666184 | 1.76274717438903 | 0.00000000034994 |
| 14 | 241259966794 | 1.76274717409913 | 0.00000000006004 |
| 15 | 1406166134592 | 1.76274717404939 | 0.00000000001030 |
| 16 | 8195736840770 | 1.76274717404085 | 0.00000000000177 |
| 17 | 47768254910040 | 1.76274717403939 | 0.00000000000030 |
| 18 | 278413792619482 | 1.76274717403914 | 0.00000000000005 |
| 19 | 1622714500806864 | 1.76274717403910 | 0.00000000000001 |
| 20 | 9457873212221714 | 1.76274717403908 | 0.00000000000000 |

TABLE 5.1

Convergence of the entropy estimate λ^\dagger in (5.1) towards the exact topological entropy $\lambda = 2\log(1 + \sqrt{2}) = 1.762747174039086\dots$ for the silver braid $\sigma_1\sigma_3\sigma_2^{-1}\sigma_4^{-1}$. Convergence appears to be exponential for a pseudo-Anosov braid, with approximately one extra digit per iteration [16].

$0 \leq x, y < 1$. The period is T , with the velocity field given by $(\sin 2\pi y, 0)$ for $0 \leq t < T/2$ and $(0, \sin 2\pi x)$ for $T/2 \leq t < T$, with t marking time. This simple flow has been well studied because the parameter range $0 \leq T \lesssim 2$ gives rich dynamics that vary from complete integrability to almost global chaos (with few visible islands in a Poincaré section).

Since the flow is piecewise steady it is easy to construct a map to track the motion of points from one period to the next. Consequently, the entropy of the flow for a given T can be found quickly and simply by direct numerical simulation of line stretching. Once the entropy of the flow is known, it is instructive to see what prediction of the entropy is given by considering the braiding of a finite number of particle orbits.

For general T it is difficult to locate unstable periodic orbits due to the highly chaotic nature of the sine mapping; however, for the special parameter $T = 1$ it is quite easy to spot some of the low order orbits. In particular, four period-two orbits are given by $\{(0, \frac{1}{4}), (\frac{1}{2}, \frac{1}{4})\}$, $\{(\frac{1}{2}, \frac{3}{4}), (1, \frac{3}{4})\}$, $\{(\frac{1}{4}, 0), (\frac{1}{4}, \frac{1}{2})\}$, and $\{(\frac{3}{4}, \frac{1}{2}), (\frac{3}{4}, 1)\}$. The first pair of orbits is depicted in Figure 5.1(a), the second pair in Figure 5.1(b). The points associated with the first pair of periodic orbits do not move in the second half-period, while those associated with the second pair do not move in the first half-period.

Now we must determine the braid formed by the eight trajectories forming these four periodic orbits. We first disambiguate the order of the periodic points by displacing them slightly along the x axis, as shown in Figure 5.2. Then we encode the trajectories in terms of braid group generators, deforming as needed. Deforming is

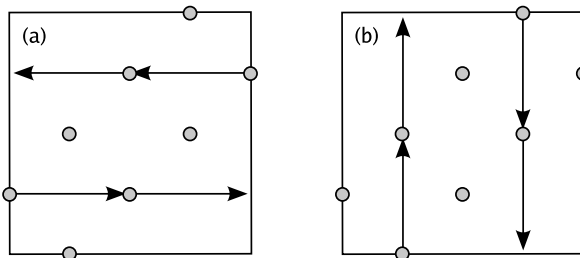


FIG. 5.1. *The four periodic orbits considered for the sine flow with $T = 1$. (a) $\{(0, \frac{1}{4}), (\frac{1}{2}, \frac{1}{4})\}$ and $\{(\frac{1}{2}, \frac{3}{4}), (1, \frac{3}{4})\}$; (b) $\{(\frac{1}{4}, 0), (\frac{1}{4}, \frac{1}{2})\}$ and $\{(\frac{3}{4}, \frac{1}{2}), (\frac{3}{4}, 1)\}$.*

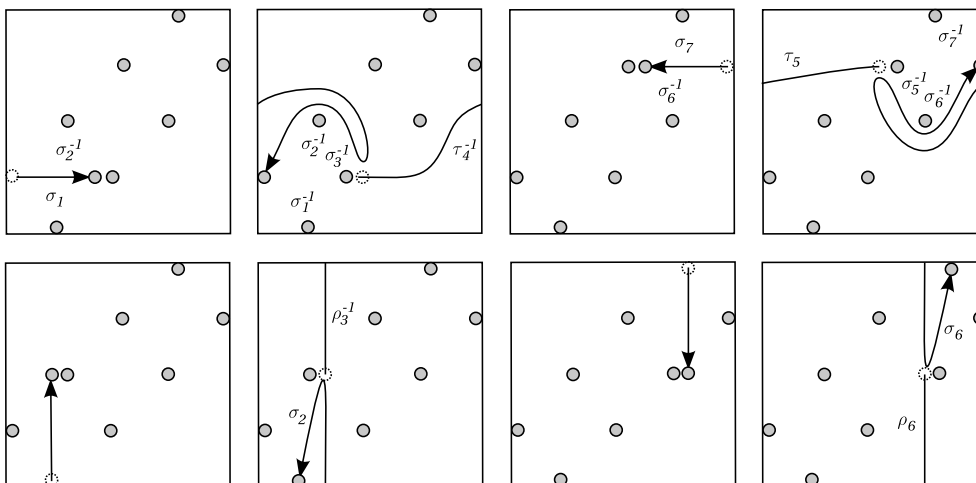


FIG. 5.2. *Illustration of the eight strand braid formed by a set of period two points in the sine flow with $T = 1$. The braid word is $\sigma_1 \sigma_2^{-1} \tau_4^{-1} \sigma_3^{-1} \sigma_2^{-1} \sigma_1^{-1} \sigma_7 \sigma_6^{-1} \tau_5 \sigma_5^{-1} \sigma_6^{-1} \sigma_7^{-1} \rho_3^{-1} \sigma_2 \rho_6 \sigma_6$. This braid has been shown to have an exact entropy of $1.21875572687\dots$ using train-tracks [10]. The entropy estimate using the growth of laminations agrees to every decimal place calculated.*

necessary since usually the trajectory does not map directly onto a generator, and some intermediate operations must be inserted. For instance, in the second snapshot in Figure 5.2 the generators $\sigma_3^{-1} \sigma_2^{-1} \sigma_1^{-1}$ are used to return the point to the leftmost position after a τ_4^{-1} operation. After a full period, the resulting braid word is $\sigma_1 \sigma_2^{-1} \tau_4^{-1} \sigma_3^{-1} \sigma_2^{-1} \sigma_1^{-1} \sigma_7 \sigma_6^{-1} \tau_5 \sigma_5^{-1} \sigma_6^{-1} \sigma_7^{-1} \rho_3^{-1} \sigma_2 \rho_6 \sigma_6$. Using equation (5.1) we find the entropy of the braid converges to $1.21875572687\dots$, which agrees with an alternative calculation using train-tracks [10]. The entropy lower bound given by the braid accounts for 82% of the flow entropy of approximately 1.48.

Since it is difficult to find any exact periodic orbits for general T it is natural to ask whether the entropy can be found by considering the braiding of any selection of trajectories. Since point motions in the sine flow are piecewise horizontal and vertical, and, for the purposes of braiding, can be performed sequentially, it is very easy and computationally fast to calculate all the σ , ρ and τ operations that occur during each half-period of the flow, for an arbitrary number of points.

For the first half-period, where all motions are horizontal, we record a σ operation

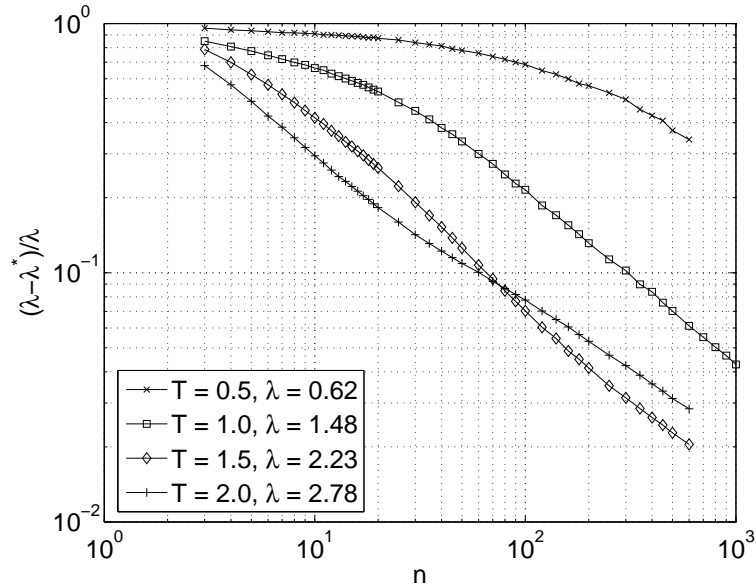


FIG. 5.3. Convergence of the mean entropy estimate $\langle \lambda^\dagger \rangle$ towards the exact entropy λ as the number of trajectories n in the braid is increased. For large n the error appears to decrease according to a power law. For smaller T the convergence is hindered by many of the points being inside periodic islands.

for each change in order of the particle x coordinates. The sign of each crossing is determined by the difference in y coordinates for the two points that cross. Special attention is required when a point crosses the periodic boundary. Crossing leftwards over $x = 0$ is achieved by $\tau_1 \sigma_1^{-1} \cdots \sigma_{n-1}^{-1}$; this moves the leftmost point one copy of the domain to the left, and then, through a sequence of σ operations, moves the point to position n and undoes all the undesired crossings with the other points. Similarly, when the rightmost point crosses over $x = 1$ the string $\tau_n^{-1} \sigma_{n-1}^{-1} \cdots \sigma_1^{-1}$ is assigned. The computation is simpler during the second half-period: all point motions are vertical, so no σ motions occur. If the i th point in the x direction crosses downwards through $y = 0$ this is labelled ρ_i . Likewise, an upwards crossing of $y = 1$ is assigned ρ_i^{-1} .

To estimate the entropy of the flow we evolve a lamination according to the braid that results from the point motions. Since the points are not periodic, the growth per iteration continues to vary, but the average value of the growth always converges. The initial points are chosen at random throughout the domain, and can either live in a chaotic region or in a periodic island. Hence the predicted entropy for a given number of points may depend on the initial positions. To allow for this we use an estimate $\langle \lambda^\dagger \rangle$ obtained by averaging over many realizations with different initial points.

In Figure 5.3 we show how the braid entropy $\langle \lambda^\dagger \rangle$ converges towards the flow entropy λ as the number of trajectories in the braid is increased. For the four different values of T we have considered, convergence appears to be as a power law for large n . Although we are unable to prove that the exact entropy is reached in the limit as $n \rightarrow \infty$ we would expect this since in this limit the braid will contain perfect information about the flow. For small values of T (such as $T = 0.5$ in Figure 5.3) the flow contains

large islands of regularity which do not contribute greatly to line stretching. In this regime n has to become relatively large before there are enough points exploring and encoding the dynamics in the small chaotic region.

Owing to the efficiency with which the braid is determined and analyzed, we are able to consider much larger times and number of points n than has been considered in previous articles [18]. Another point worth noting is that for $T = 1$, the mean entropy estimate $\langle \lambda^\dagger \rangle = 0.45$ with $n = 8$ eight points is much worse than the estimate of $\lambda^\dagger = 1.22$ found by using the set of eight judiciously chosen periodic points considered earlier. This highlights the important role of low order periodic orbits in determining much of the nature of the flow.

6. Discussion. We have derived a dynamical system to compute the evolution of a lamination (equivalence class of simple closed curves) under the braiding of an arbitrary number of punctures on the torus. The method is essentially a modification of the Dynnikov coordinate approach employed by Moussafir [16], but we use a triangulation encoding that has favorable properties for studying torus braids. Naturally, our method also works for the special cases of cylinder and planar braids. However, in the planar case our dynamical system still has $3n$ variables, more than the $2n - 3$ required by Moussafir, so there is clearly some redundancy in this case. Also, the triangulation of our domain is not unique, so we expect that the details of our method are not unique. However our triangulation seems to be the best choice for simplifying the arithmetic.

For completeness we point out that our dynamical system does not work directly for $n = 2$ punctures because in equation (3.3) and (3.4) this would mean that the indices $i - 1$ and $i + 1$ refer to the same quantities. There is nothing difficult about the case $n = 2$ though, and in principle one could write down the corrected update rules for $\{x_1, y_1, z_1, x_2, y_2, z_2\}$. Alternatively, a lazy but convenient workaround is to include a redundant third puncture, glued to one of the other two, so that it is slaved to its motion. At a little more computational expense this allows one computer code to handle all values of $n \geq 2$. The case $n = 1$ is trivial.

By using similar arguments to Moussafir [16], it can be shown that as the number of iterations tends to infinity the logarithm of the number of lamination crossings grows at the rate of the braid topological entropy. Though the number of crossings grows exponentially fast, our numerical implementation of the dynamical system uses a large integer arithmetic library to allow calculation of the entropy to arbitrary precision. Convergence appears to be exponentially fast, with approximately one digit of accuracy gained per iteration for the braids we have considered.

In practice, if only a few digits of accuracy are required then double precision floating-point arithmetic for the crossing numbers is adequate and can speed up code significantly. A caveat with using floating-point arithmetic is that it destroys reversibility. In general by performing a long braid followed by its inverse the initial lamination will not be recovered due to exponential growth of small roundoff errors. This is akin to irreversibility due to numerical diffusion in trajectory computations in a chaotic Stokes flow. However, since the dynamical system itself is exact, the only errors are due to roundoff and not to discretization, so even with double precision the dynamical system is surprisingly reversible.

If finite precision is not acceptable, our method is easily adapted to find exact entropies. This can be done by shortcircuiting the minimum functions in the update rules (3.1)–(3.4). Under repeated application of a braid, the dynamical system quickly converges to a periodic pattern where it is known in advance which number will be taken for each minimum. With this knowledge each call to the min function can be replaced by the correct variable and then a linear system can be written down for the crossing numbers. The logarithm of the modulus of the largest eigenvalue will give the exact entropy.

This work was motivated by the study of two-dimensional fluid mixing via the braiding motion of fluid particle trajectories [11,18]. In this setting we have derived an efficient tool that allows practical analysis of large braids. Outside of this particular application it is natural to ask whether the method can be generalized for the braid group on surfaces of higher genus, as considered by Birman [3]. Since any surface can be triangulated, in principle our method could be extended to higher genus. The problem anticipated with generalizing the approach is that it is more difficult to visualize the preimage problems on a surface with many holes, and also it is not clear in general how to exploit group properties to gain a complete set of crossing update rules.

We thank Colin Cotter and Jacques-Oliver Moussafir for helpful discussions. This work was funded by the UK Engineering and Physical Sciences Research Council grant GR/S72931/01.

REFERENCES

- [1] H. AREF, *The development of chaotic advection*, Phys. Fluids, 14 (2002), pp. 1315–1325.
- [2] M. BESTVINA AND M. HANDEL, *Train-tracks for surface homeomorphisms*, Topology, 34 (1995), pp. 109–140.
- [3] J. S. BIRMAN, *On braid groups*, Comm. Pure Appl. Math., 22 (1969), pp. 41–72.
- [4] P. L. BOYLAND, *Topological methods in surface dynamics*, Topology Appl., 58 (1994), pp. 223–298.
- [5] P. L. BOYLAND, H. AREF, AND M. A. STREMLER, *Topological fluid mechanics of stirring*, J. Fluid Mech., 403 (2000), pp. 277–304.
- [6] D. D’ALESSANDRO, M. DAHLEH, AND I. MEZIĆ, *Control of mixing in fluid flow: A maximum entropy approach*, IEEE Trans. Automat. Control, 44 (1999), pp. 1852–1863.
- [7] I. A. DYNNIKOV, *On a Yang–Baxter map and the Dehornoy ordering*, Russian Math. Surveys, 57 (2002), pp. 592–594.
- [8] M. D. FINN, S. M. COX, AND H. M. BYRNE, *Topological chaos in inviscid and viscous mixers*, J. Fluid Mech., 493 (2003), pp. 345–361.
- [9] ———, *Mixing measures for a two-dimensional chaotic Stokes flow*, J. Eng. Math., 48 (2004), pp. 129–155.
- [10] M. D. FINN, J.-L. THIFFEAULT, AND E. GOUILLART, *Topological chaos in spatially periodic mixers*, Physica D, (2006), arXiv:nlin/0507023. in press.
- [11] J.-M. GAMBAUDO AND E. E. PÉCOU, *Dynamical cocycles with values in the Artin braid group*, Ergod. Th. Dynam. Sys., 19 (1999), pp. 627–641.
- [12] E. GOUILLART, J.-L. THIFFEAULT, AND M. D. FINN, *Topological mixing with ghost rods*, Phys. Rev. E, 73 (2006), p. 036311 (8 pages).
- [13] T. HALL, *Train: A C++ program for computing train tracks of surface homeomorphisms*. http://www.liv.ac.uk/maths/PURE/MIN_SET/CONTENT/members/T.Hall.html.
- [14] B. KOLEV, *Entropie topologique et représentation de Bureau*, C. R. Acad. Sci. Sér. I, 309 (1989), pp. 835–838. English translation available at <http://arxiv.org/abs/math.DS/0304105>.
- [15] M. LEFRANC, *Alternative determinism principle for topological analysis of chaos*. In submission, 2005, arXiv:nlin/0503006.
- [16] J.-O. MOUSSAFIR, *On the entropy of braids*. In submission, 2006, arXiv:math.DS/0603355.
- [17] S. NEWHOUSE AND T. PIGNATARO, *On the estimation of topological entropy*, J. Stat. Phys., 72 (1993), pp. 1331–1351.

- [18] J.-L. THIFFEAULT, *Measuring topological chaos*, Phys. Rev. Lett., 94 (2005), p. 084502.